Crystallochromy of perylene pigments: Influence of an enlarged polyaromatic core region

L. Gisslén[1,*] and R. Scholz[2,†]

[1]*Walter Schottky Institut und Physik Department, Technische Universität München, Am Coulombwall 3, D-85748 Garching, Germany*
[2]*Institut für Angewandte Photophysik, Technische Universität Dresden, D-01062 Dresden, Germany*

As demonstrated in a recent model study of several perylene pigments crystallizing in the monoclinic space group $P2_1/c$, the optical properties in the crystalline phase are determined by the interference between neutral molecular excitations and charge transfer states via electron and hole transfer. In the present work, we apply this exciton model to three further perylene compounds crystallizing in the space groups $P2_1/n$, $P\bar{1}$, and $P2_1/c$, involving two chromophores with an enlarged polyaromatic core. In all cases, the charge transfer between stack neighbors increases the second moment of the optical response, whereas a larger conjugated core results in a red shift of the neutral excitation energy of each chromophore.

I. INTRODUCTION

Organic crystalline materials with semiconducting properties have resulted in various electronic and optoelectronic applications, including organic field effect transistors, light-emitting diodes, and photoreceptors. For photovoltaic devices, materials with reduced absorption edge would be favorable because they could better cover the solar spectrum. Polymer-fullerene bulk heterojunctions containing a fluorene copolymer show an improved spectral response in the near infrared, but the resulting power conversion has remained rather low.[1] On the other hand, for chromophores based on perylene and related compounds, it is well established that an extension of the aromatic core tunes the absorption edge to the infrared,[2,3] and some crystalline perylene pigments show a large exciton diffusion length which might become favorable for an improved charge generation at a hetero-interface.[4,5]

Among the perylene compounds, perylene bisimides have received particular attention due to their fascinating properties. In a solution, they form aggregates with strongly modified absorption and emission properties,[6] and depending on the size and type of the sidegroups attached to the diimide groups, in the condensed phase they may result in several variants of liquid crystals[7,8] or crystals.[9–11] Dispersion-corrected density functional calculations of molecule pairs have revealed a competition between Coulomb attraction, Pauli repulsion, and dispersion interactions, allowing to understand preferential stacking geometries realized in crystalline pigments.[12]

In the solid phase, the interaction between the transition dipoles of adjacent molecules results in the transfer of neutral molecular excitations, so that periodic crystals have a well-defined excitonic band structure which can be used for a detailed assignment of absorption and photoluminescence (PL) spectra.[13,14] Moreover, in most perylene compounds, rather large electron and hole transfer parameters mix neutral molecular excitations and charge transfer (CT) states involving stack neighbors. As a result, the spectroscopic signature of small aggregates and extended crystals is strongly modified with respect to dissolved monomers,[6,15,16] a finding which can be rationalized on the basis of exciton models accounting for this coupling mechanism.[17–21] A recent extension of elementary sum rules for the transfer of neutral excitations[22,23] toward the interference between neutral excitations and CT

states has revealed that CT states play a key role for the linear optical properties of molecular crystals even though their own oscillator strength may be rather small.[21]

In the present work, we analyze three perylene pigments within the framework of an exciton model accounting for the interference between Frenkel excitons and CT states. The three molecules differ in the size of the conjugated core region, so that two out of three show a significant red shift with respect to typical perylene tetracarboxylic bisimides,[15] and one of them, PTCBI (3,4,9,10-perylenetetracarboxylic-bis-benzimidazole), has already served as a model compound for photovoltaic applications.[24–26] Section II summarizes the key features of the exciton model presented in Ref. 21, hereafter called I. In Sec. III, we present the three chromophores and their crystalline phases before proceeding to the calculation of the parameters required for the exciton model. Most of them can be computed with density functional theory (DFT) applied to monomers or stacked dimers. The transfer of neutral excitations and the energy E_{00}^{F} of the lowest vibronic subband of the monomer are derived from sum rules concerning the first and second moment of the observed highest occupied molecular orbital-lowest unoccupied molecular orbital (HOMO-LUMO) absorption band in the crystalline phase, and the difference $\Delta_{00} = E_{00}^{CT} - E_{00}^{F}$ between the lowest subbands of CT state and neutral excitation is treated as a free fitting parameter. Section IV is devoted to a comparison between the calculated and observed linear optical spectra, and Sec. V summarizes our main findings.

II. EXCITON MODEL

The localized excitations included in our exciton model are visualized in Fig. 1, compare I (Ref. 21). An optical excitation of site n as visualized in the central column of Fig. 1 can be achieved with the rather large transition dipole μ_F of the molecular HOMO-LUMO transition, whereas for the six compounds investigated previously, the CT states have an oscillator strength about two orders of magnitude smaller according to a much smaller transition dipole $\mu_{CT} \ll \mu_F$.[21]

The coupling between the transition dipoles on different sites allows the transfer of neutral excitations between different molecules. Therefore, the Bloch waves of neutral molecular
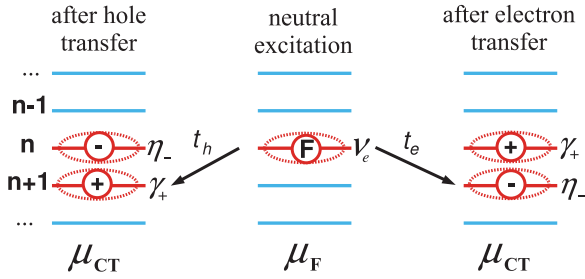
FIG. 1. (Color online) Localized excitations in a one-dimensional stack of molecules. Center: neutral molecular excitation on site n; left: CT state obtained from the neutral excitation after transferring a hole from site n to site $n+1$; right: CT state after transferring an electron from site n to site $n+1$. The vibronic levels of the cationic, anionic, or neutral excited states are indicated as γ_+, η_-, and ν_e, respectively.

excitations will have an energy depending on their wave vector, defining a bosonic dispersion relation for so-called Frenkel excitons.[13,14] Moreover, as shown in Fig. 1, neutral molecular excitations interfere with CT states via electron transfer t_e and hole transfer t_h between stack neighbors. Each excited or ionized molecule has to be treated with the levels of an effective internal vibration $\hbar\omega$, and the respective arguments of the Poisson progression over the vibronic levels are called S_+ for a cationic state, S_- for an anionic state, and S for a neutral excited molecule.

In the crystal ground state, all molecules remain in the lowest level of the effective internal vibration. The vibronic basis states in Fig. 1 included in our exciton model are restricted to the ones carrying oscillator strength for excitation from the crystal ground state, as opposed to dark states containing a vibronic excitation on a molecule in its electronic ground state together with an electronic and vibronic excitation on a different site. In specific cases these dark states may have a substantial influence on the absorption and emission spectra,[27] including the splitting between the lowest vibronic levels of the absorption line shape.[20] As the present work concentrates on the influence of CT states on a modification of the optical response, additional complications arising from the mixing between dipole-allowed transitions and dark states will be ignored.

Due to the smallness of their transition dipoles, on first sight the CT states seem to be irrelevant for the optical response of a molecular crystal. Albeit, in the limit of vanishing transition dipole of the CT states, an analysis of the lowest moments of the optical response of the Frenkel-CT model reveals that the sheer presence of the CT states results in an increase of the second moment of the imaginary part of the dielectric function

$$\langle(\Delta E)^2\rangle = S(\hbar\omega)^2 + 2(t_e + t_h)^2, \tag{1}$$

irrespective of the position of their lowest vibronic level E_{00}^{CT} with respect to the fundamental E_{00}^{F} of the neutral excitation, compare I (Ref. 21). On the other hand, the CT states have no influence on the first moment

$$\langle E\rangle = E_{00}^{\mathrm{F}} + S\hbar\omega + T, \tag{2}$$

determined exclusively by neutral molecular excitations and the excitonic transfer parameter T at the Γ point of the Brillouin zone, or $\mathbf{k} = \mathbf{0}$, so that the average transition energy still

coincides with a pure Frenkel exciton model.[21–23] Therefore, both the lowest sublevel E_{00}^{F} of a neutral excitation in the crystalline phase and the exciton transfer T can be derived in a controlled way from the average over the imaginary part of the observed dielectric function. In crystals with two basis molecules A and B, the exciton transfer has to be generalized to transfer from basis molecule A to the same basis molecule in all other cells, called T_{AA}, and transfer from basis molecule A to all basis molecules B, called T_{AB}. In these cases, the transfer matrix element T entering the sum rule in Eq. (2) has to be replaced by $T = T_{AA} \pm T_{AB}$. Further details of the exciton Hamiltonian can be found in I (Ref. 21).

III. MODEL COMPOUNDS

A. Geometry and crystal structure

The molecular crystals investigated in this work are composed of 5,15-diaza-6,16,dihydroxy-tetrabenzo [*b*,*e*,*k*,*n*]perylene (DDTP), 3,4,9,10-perylenetetracarboxylic-bis-benzimidazole (*trans* isomer of PTCBI), and N,N'-di-*n*-butylperylene-3,4:9,10-bis(dicarboximide) (BP), compare Fig. 2.

In the DDTP molecule, the perylene core is extended by additional hexagonal rings attached to each corner of the perylene core. As the hydrogen atoms of these groups repell each other, the molecule reduces its elastic energy by bending adjacent rings out of the plane of the perylene core. The planarity of the central region of DDTP is stabilized by two OH groups attached in the bay region of the perylene core, so that they form internal hydrogen bridges with the adjacent nitrogen atoms. The resulting geometry resembles two nonplanar pentacene molecules crossing each other at an angle of 60°, one functionalized with two OH groups, the other
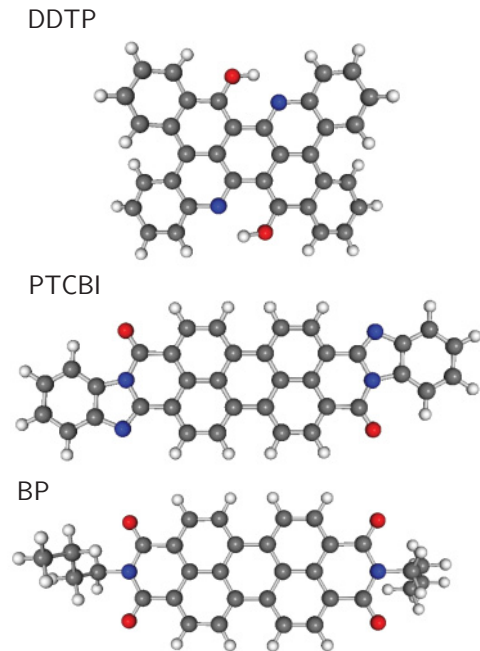

FIG. 2. (Color online) Compounds studied in the present work, from top to bottom: DDTP ($C_{34}O_2N_2H_{18}$), *trans*-PTCBI ($C_{36}O_2N_4H_{16}$), and BP ($C_{32}O_4N_2H_{26}$).

TABLE I. Crystal structures for the three model compounds, ordered according to the length of the stacking vector ($\boldsymbol{a}$ for PTCBI and BP, $\boldsymbol{b}$ for DDTP). In the monoclinic space groups $P2_1/c$ and $P2_1/n$, the lattice vector $\boldsymbol{b}$ is orthogonal to the other two, $\boldsymbol{a} \perp \boldsymbol{b} \perp \boldsymbol{c}$. V_0 the volume of the unit cell, and Z the number of basis molecules.

Compound	Space group	a Å	b Å	c Å	V_0 Å^3	Z 1
DDTP (Ref. [28])	$P2_1/n$	10.559	**3.775**	26.517	1056.7	2
PTCBI (Ref. [29])	$P\bar{1}$	**4.729**	8.282	14.693	556.2	1
BP (Ref. [9])	$P2_1/c$	**4.734**	28.233	9.396	1173.5	2

with two nitrogen ones. In PTCBI, an extension of the perylene core is obtained by a functionalization with two benzimidazole groups.

In contrast to BP crystallizing in the monoclinic space group $P2_1/c$ occurring for several perylene bis(carboximide) compounds,[9] both DDTP and PTCBI prefer different space groups, compare Table I. In all cases, the intermolecular distance measured along the molecular normal remains much smaller than the length of the stacking vector. As a result, the stacking vector produces substantial projections onto the long and short axes of the perylene core. From a comparison of the projections in Table II with the geometry of other perylene pigments, we deduce that DDTP realizes a stacking geometry similar to PTCDA (3,4,9,10-perylene tetracarboxylic dianhydride) and Me-PTCDI (N,N'-dimethyl-3,4,9,10-perylene tetracarboxylic diimide), whereas PTCBI and BP resemble merely PTCDI (3,4,9,10-perylenetetracarboxylic diimide) and the black pigment PB31 (Ref. [21]). In a recent investigation of the influence of dispersion interactions onto the cohesive energy of two PTCDI molecules, it was realized that these two types of stacking geometries are indeed particularly favorable.[12]

B. Optical properties of thin films

In Fig. 3, we compare the optical densities of the three compounds under study. BP shows a highly structured optical response with several well resolved vibronic features. Similar to Me-PTCDI and PB31, the height of subsequent subbands is a nonmonotonous function of energy, so that the absorption band breaks into two separated regions with maxima at 2.10 and 2.67 eV. The lowest subband falls into the energy range 2.01 to 2.19 eV observed for other perylene bis(carboximides), compare I. Both in DDTP and in PTCBI, the lowest subband is significantly redshifted. As will be discussed below in more detail, this redshift results from the larger extension of the

TABLE II. Geometric arrangement of chromophores with respect to each other: lattice vector along the stacking direction, and projections into the Cartesian reference frame of the molecule defined by its long axis, short axis, and molecular normal.

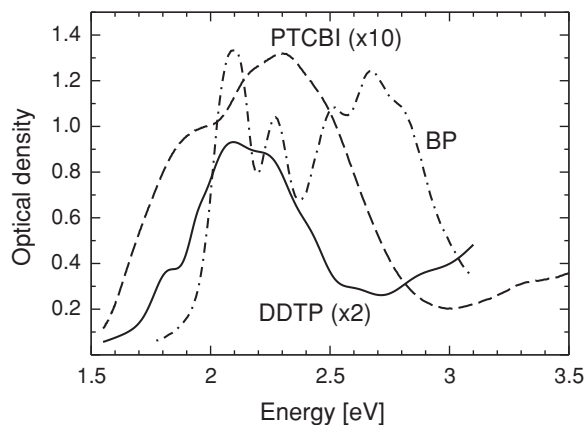| Compound	Stack Å	Long Å	Short Å	Normal Å
DDTP	3.775	0.42	1.49	3.44
PTCBI	4.729	3.15	1.04	3.36
BP	4.734	3.11	1.03	3.42

FIG. 3. Optical density of DDTP at $T = 12$ K (solid line, film thickness 80 nm, multiplied by 2),[30] *trans* PTCBI at room temperature (dashed, film thickness 15 nm, multiplied by 10),[31,32] and BP at $T = 20$ K (dash-dotted, film thickness 100 nm).[37]

polyaromatic core in each monomer and additional solid state effects.

C. HOMO-LUMO transition

In the present work, the molecular orbitals are calculated with the hybrid functional Becke, three-parameter, Lee-Yang-Parr (B3LYP),[33] and transition energies with time-dependent DFT (TD-DFT) using the same functional. For the electronic orbitals and the transition energies, we use a well converged triple-ζ variational basis including polarization functions (TZVP).[34] All calculations are performed with the TURBOMOLE 5.9 program package.[35]

The frontier orbitals of DDTP in Fig. 4 reveal an extension over the entire polyaromatic area, with some resemblence to the HOMO and the LUMO of pentacene. Due to the more extended frontier orbitals, it can be expected that the dipole-allowed HOMO-LUMO transition of DDTP should be redshifted with respect to a typical perylene bis(dicarboximide) like BP, as observed for the dissolved molecules, compare Table III.

In the frontier orbitals of *trans* PTCBI shown in Fig. 5, the node patterns in the core resemble other perylene compounds, but the extension over the benzimidazole groups produces a redshift of the HOMO-LUMO transition with respect to perylene diimides like BP, compare Table III. The TD-DFT transition energies at the B3LYP/TZVP level reproduce the redshift of PTCBI with respect to BP, but the even larger redshift of DDTP with respect to BP cannot be obtained.
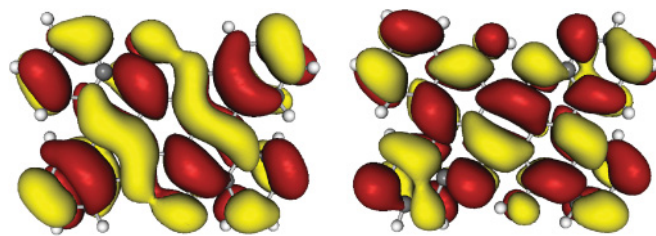

FIG. 4. (Color online) Frontier orbitals of DDTP in the nonplanar geometry realized in the crystalline phase: HOMO (left) and LUMO (right).

TABLE III. Fundamental transition E_{00} observed for chromophores dissolved in dimethylsulfoxide and lowest dipole-allowed transition energy E obtained with time-dependent DFT at the B3LYP/TZVP level, together with its transition dipole μ (Debye) and oscillator strength f_{osc}.

Compound	E_{00} eV	E eV	μ D	f_{osc} 1
DDTP	1.97 (Ref. 30)	2.55	7.26	0.510
PTCBI	2.06 (Ref. 36)	2.01	11.85	1.070
BP	2.36 (Ref. 37)	2.39	8.87	0.712

Presumably, the failure of a well-tested method for the lowest transition of DDTP can be related to internal charge transfer between the two inequivalent pentacene-like moieties, so that the energies of the Kohn-Sham orbitals and the transition energies obtained with TD-DFT are influenced by the wrong asymptotics of the exchange functional deviating from $-1/r$.

D. Huang-Rhys factors

The geometry of a molecule depends on its electronic configuration, so that the shapes in the electronic ground state, the neutral excited state, and the cationic or anionic configurations will differ. As discussed previously for other perylene compounds, the neutral excited state optimized under the constraint of the nonequilibrium occupations $n_{\text{HOMO}} = n_{\text{LUMO}} = 1$ of the frontier orbitals gives a more reliable deformation pattern than an optimization with TD-DFT, compare I (Ref. 21). Each deformation pattern is projected onto the eigenvectors of the internal vibrations $\hbar\omega_k$, defining in turn a contribution λ_k to the reorganization energy and a Huang-Rhys factor S_k according to

$$\lambda_k = S_k \hbar \omega_k. \qquad (3)$$

By averaging over the internal vibrations in the region from 900 to 1700 cm^{-1}, we obtain an *effective* internal mode at $\hbar\omega$ with a Huang-Rhys factor S. The individual Huang-Rhys factors S_k are visualized in Fig. 6, and the Huang-Rhys factors S of the effective internal mode are tabulated in Table IV. The mode frequencies have been scaled by a factor of 0.973 adequate for the B3LYP functional[38] and the Huang-Rhys factors by 1/0.973.

E. Electron transfer and hole transfer

As discussed in Sec. II, a key feature of our exciton model is the interference between Frenkel excitons and CT states via electron transfer t_e and hole transfer t_h. These parameters can be obtained from a DFT calculation of a stacked dimer
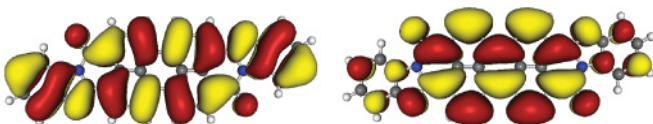

FIG. 5. (Color online) Frontier orbitals of *trans* PTCBI in the geometry realized in the crystalline phase: HOMO (left) and LUMO (right).
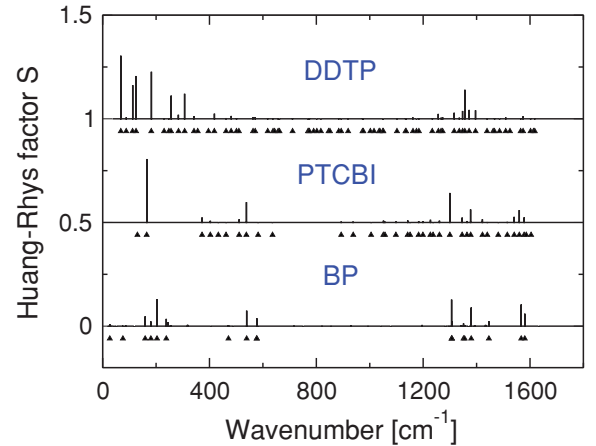

FIG. 6. (Color online) Huang-Rhys factors for neutral excitation of the three perylene compounds, obtained from a projection of the deformation in the relaxed excited geometry onto the eigenvectors of the internal vibrations. The relaxed excited geometry has been calculated at the B3LYP/TZVP level under the constraint $n_{\text{HOMO}} = n_{\text{LUMO}} = 1$, and the vibrational eigenvectors at the B3LYP/DZ (double-ζ) level. For clarity, the baselines applying to different compounds are shifted.

in a geometry compatible with the crystalline phase, compare Table V.

For PTCBI and BP, the hole transfer t_h dominates, with a value in the same range as for PTCDI and PB31, a correspondence related to a similar stacking geometry, compare I. In DDTP, even though the stacking geometry resembles Me-PTCDI, the transfer parameters of these two compounds differ substantially because the frontier orbitals of DDTP do no more follow the typical node patterns observed for various perylene carboxylic diimides and for diindenoperylene.[16] As opposed to Me-PTCDI with $|t_e| > |t_h|$, in DDTP the hole transfer t_h is much larger in absolute than the electron transfer t_e.

IV. RESULTS

A. Data analysis

For monoclinic and triclinic space groups, the full determination of the real and imaginary part of the dielectric

TABLE IV. Effective internal vibration for the three perylene compounds, with Huang-Rhys factors S_+ and S_- deduced from the cationic or anionic configurations, and Huang-Rhys factor S in the relaxed excited geometry obtained with DFT under the constraint $n_{\text{HOMO}} = n_{\text{LUMO}} = 1$ (c-DFT), and with TD-DFT. All geometry optimizations have been calculated at the B3LYP/TZVP level, and the vibrational modes with B3LYP/DZ.

Compound	Mode $\hbar\omega$ eV	Cation S_+ 1	Anion S_- 1	Excited c-DFT S 1	Excited TD-DFT S 1
DDTP	0.167	0.38	0.46	0.72	0.49
PTCBI	0.171	0.29	0.49	0.77	0.48
BP	0.175	0.30	0.57	0.82	0.52

TABLE V. Transfer parameters t_h and t_e obtained from a B3LYP/TZVP calculation of a stacked dimer compatible with the crystal geometry.

Compound	t_h eV	t_e eV
DDTP	−0.108	0.028
PTCBI	0.174	−0.018
BP	0.139	0.018

TABLE VI. Parameters of the Frenkel-CT model, with $\Delta_{00} = E_{00}^{CT} - E_{00}^{F}$. The intramolecular deformation parameters are chosen according to Table IV. For each compound, the tabulated value of E_{00}^{F} contains already a suitable gas-to-crystal shift.

Compound	T K	E_{00}^{F} eV	E_{00}^{CT} eV	Δ_{00} eV	T_{AA} eV	T_{AB} eV	t_h eV	t_e eV	μ D
DDTP	12	1.89	1.87	−0.02	0.15	0.00	−0.090	0.044	4.13
PTCBI	300	1.91	1.99	0.08	0.13	-	0.174	−0.018	4.46
BP	20	2.26	2.32	0.06	0.03	0.00	0.142	0.027	6.10

tensor requires techniques like spectroscopic ellipsometry performed on several facets of a macroscopic sample. As this comprehensive information is only available in exceptional cases,[39] we have analyzed the optical density of polycrstalline thin films of the three perylene compounds displayed in Fig. 3. The refractive index is modeled with a Kramers-Kronig consistent function where the imaginary part is composed of several Gaussian subbands, and the real part includes a dispersive background arising from transitions at higher energy. In the organic thin film, multiple interferences are included with a transfer matrix formalism generalized to a complex refractive index. We have also allowed for a possible offset of the published optical density spectra, which may have been used for suppressing the apparent optical density arising from reflectivity losses in the transparent region of the organic material. In regions where no optical transition takes place, scattering losses and nonspecular reflection may contribute to a finite value of the optical density. Our thin film model does not account for such loss mechanisms, so that the fitting procedure gives an upper limit for the imaginary part of the refractive index.

As the optical density is mainly determined by the imaginary part of the refractive index, our data analysis introduces some arbitrariness for the background value of the real part of the refractive index. Hence, in the resulting imaginary part of the dielectric function $\mathrm{Im}(\epsilon) = 2\mathrm{Re}(n)\Im(n)$, the ratio between the areas of the highest and lowest vibronic subbands may be influenced by up to 20%.

B. Parameters of exciton model

The parametrization of the exciton model relies on the imaginary part of the dielectric function derived from the measured optical density, resulting in the values summarized in Table VI. The lowest subband E_{00}^{F} of the neutral molecular excitation is redshifted by 0.08 to 0.15 eV with respect to dissolved molecules, indicating that the gas-to-crystal shift is substantially larger than the gas-to-solute shift, a trend observed also for other perylene compounds like PTCDA and Me-PTCDI. As the energy of the lowest vibronic subband contributing to the optical response is modified by exciton transfer and the strong interactions with the CT states, a suitable value for E_{00}^{F} in the crystalline phase is somewhat larger than the energy of the lowest observed feature.

As the sum rule for the second moment in Eq. (1) does not depend on the position of the lowest vibronic subband E_{00}^{CT}, this parameter is varied until the best agreement between calculated and measured optical line shape is obtained. The difference $\Delta_{00} = E_{00}^{CT} - E_{00}^{F}$ is displayed in Fig. 7. As expected for the

model of a condensator consisting of two parallel plates, the relative energy position of the CT state follows approximately a linear slope as a function of the length $l = a$ or $l = b$ of the stacking vector, with $d\Delta_{00}/dl \approx 0.08$ eV/Å.

Electron and hole transfer parameters close to the B3LYP/TZVP values in Table V yield an excellent agreement with the observed refractive index, see Secs. IV C to IV E for a detailed comparison of calculated and observed line shapes. The average absolute deviation between the values for t_h and t_e in Tables V and VI remains as small as 8 meV, in the same range as the average absolute deviation of 10 meV obtained for the the six compounds studied in I (Ref. 21).

The transition dipoles in Table VI are obtained from the area under the imaginary part of the dielectric function derived from a fit to the optical density and a comparison between calculated and experimentally determined line shapes. For thin films of BP, the ratio $\mu_{\mathrm{fit}}^2/\mu_{\mathrm{TD-DFT}}^2$ between the transition strength fitted to the observed optical density in Fig. 3 and the respective value in Table III is 0.47, indicating that both basis molecules in the unit cell have their transition dipoles close to parallel to the substrate plane. In DDTP, this ratio drops to 0.32, close to the value of 1/3 expected for random orientation of the transition dipoles with respect to the substrate orientation. In
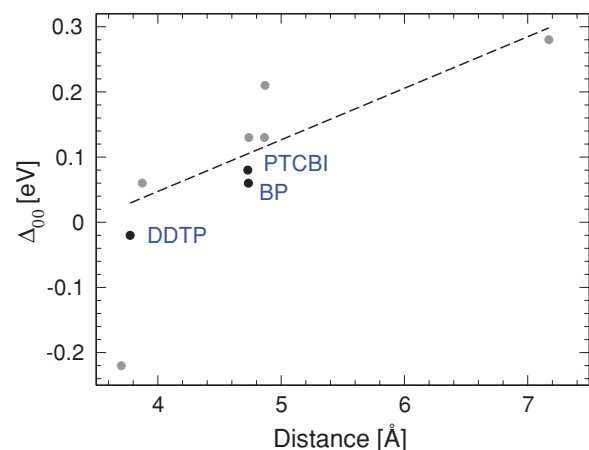

FIG. 7. (Color online) Dependence of the difference between the lowest vibronic subbands of the CT transition and the neutral molecular excitation $\Delta_{00} = E_{00}^{CT} - E_{00}^{F}$ on the length of the stacking vector. Gray dots represent the six perylene compounds studied previously, and black dots the three compounds DDTP, *trans* PTCBI, and BP. A linear slope (dashed line) is fitted through the values for eight compounds excluding PTCDA (smallest stacking vector and lowest value Δ_{00}).
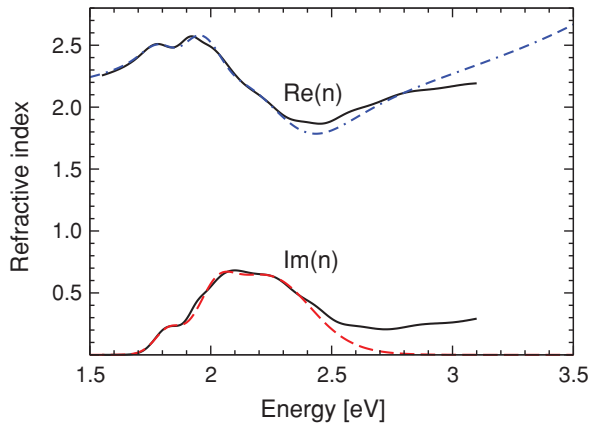
FIG. 8. (Color online) Refractive index of DDTP: Kramers-Kronig consistent fit to observed optical density (black), and model calculation for Re(n) (blue dash-dotted) and Im(n) (red dashed).
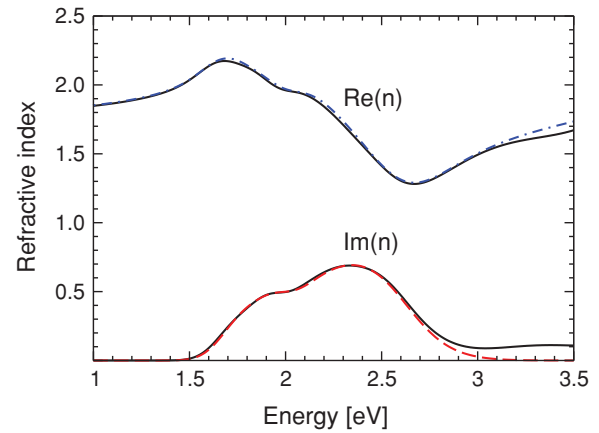

FIG. 9. (Color online) Refractive index of *trans* PTCBI: Kramers-Kronig consistent fit to observed optical density (black), and model calculation for Re(n) (blue dash-dotted) and Im(n) (red dashed).

the fit of the optical density of *trans* PTCBI, this ratio is only 0.14, compatible with transition dipoles oriented preferentially along the substrate normal.

C. DDTP

In DDTP, the mixing between Frenkel and CT states pushes the lowest subband to about 1.82 eV, somewhat below $E_{00}^F = 1.89$ eV and $E_{00}^{CT} = 1.87$ eV, compare Fig. 8. This onset of the HOMO-LUMO transition band is significantly below the values of 2.01 to 2.25 eV observed for the six perylene compounds studied in I. Moreover, the fact that Frenkel and CT excitations are close to resonant avoids substantial activation barriers between the lowest strongly absorbing subband and the threshold energy allowing for the separation of optically excited states into an electron hole pair delocalized over two stack neighbors. Therefore, DDTP combines two favorable properties for photovoltaic applications: First, the lower onset of absorption covers the solar spectrum in a better way than the perylene compounds studied in I, and second, the creation of a localized electron hole pair should have a smaller activation barrier.

D. *trans* PTCBI

In the optical spectra of *trans* PTCBI displayed in Fig. 9, the lowest vibronic subband of the HOMO-LUMO transition is located at 1.76 eV. Due to the substantial Gaussian broadening, the absorption starts already at 1.5 eV, so that this material is particularly suited for photovoltaic applications.[24–26] In a comparison between PTCBI films composed of *cis* isomers, *trans* isomers, or a mixture of both, it turned out that the *trans* isomer is best suited for photovoltaic cells: The redshifted onset of the optical absorption produces an increased efficiency in a bilayer solar cell.[31] The moderate difference $\Delta_{00} = E_{00}^{CT} - E_{00}^F = 0.08$ eV and the substantial mixing between Frenkel excitons and CT states should allow to ionize an optical excitation of the lowest subband at 1.76 eV into a charge pair residing on two stack neighbors. As discussed previously for PTCDA, a separation of this localized CT state into a free electron hole pair may require a substantial energy of the order of 1 eV (Ref. 40), so that charge separation at a heterointerface

in a bilayer solar cells or in a bulk heterojunction seems to be a more promising device application.[31,41]

E. BP

As shown in Figs. 3 and 10, the optical response of BP shows rather narrow vibronic subbands. Similarly to other perylene diimides like Me-PTCDI, PTCDI, and PB31, the intensities of consecutive subbands follow a nonmonotonous function of energy, giving instead two major absorption peaks around 2.10 and 2.67 eV surrounding a valley region. As discussed already in I, this is a signature of a large electron or hole transfer parameter, breaking the HOMO-LUMO absorption band into two major components.

In the crystalline phase, the butyl groups are bended out of the plane of the polyaromatic core region, so that their presence has little influence on the energy of the HOMO-LUMO transition. Among all nine perylene compounds studied in the present work and in I, BP shows the largest transition energy $E_{00}^F = 2.26$ eV, indicating a particularly small gas-to-crystal shift. Nevertheless, the substantial mixing between Frenkel excitons and CT states pushes the lowest vibronic band down to 2.10 eV, a value resembling PTCDI and Me-PTCDI.[21]
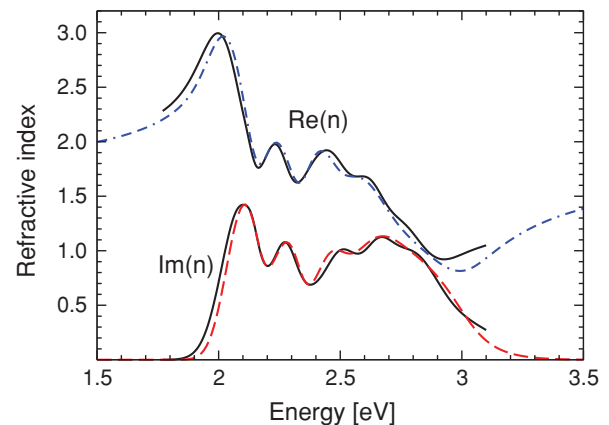

FIG. 10. (Color online) Refractive index of BP: Kramers-Kronig consistent fit to observed optical density (black), and model calculation for Re(n) (blue dash-dotted) and Im(n) (red dashed).

According to Fig. 7, the fitted difference $\Delta_{00} = E_{00}^{CT} - E_{00}^{F} = 0.06$ eV is somewhat smaller than in other pigments with similar stacking geometry, so that the photogeneration of electron hole pairs localized on stack neighbors should not be inhibited by a large activation barrier. As mentioned already for *trans* PTCBI, the large Coulomb attraction between an electron and a hole residing on stack neighbors may induce a large activation barrier for the generation of a free electron hole pair. Therefore, the relatively low-lying CT energy might become useful for photodetectors under large bias voltage or for efficient charge separation in bulk heterojunction solar cells.

V. CONCLUSION

In the present work, we have demonstrated the general validity of an exciton model allowing for the mixing of Frenkel excitons and CT state by applying it to three fur- ther semiconducting molecular crystals. Among the perylene pigments investigated, two contain an enlarged polyaromatic core, leading to a redshifted onset of the optical absorption with respect to perylene diimides. Hence, in photovoltaic applications, these materials can cover the solar spectrum in a more complete way. The three compounds studied have particularly low CT energies, so that optically excited states can easily evolve into localized electron hole pairs, suggesting that all three molecular materials could serve as efficient photodetectors or materials for bulk heterojunction solar cells.

*linus.gisslen@ph.tum.de

†reinhard.scholz@iapp.de

[1] X. Wang, E. Perzon, F. Oswald, F. Langa, S. Admassie, M. R. Andersson, and O. Inganäs, Adv. Funct. Mater. **15**, 1665 (2005).

[2] F. Nolde, W. Pisula, S. Müller, C. Kohl, and K. Müllen, Chem. Mater. **18**, 3715 (2006).

[3] Y. Avlasevich, S. Müller, P. Erk, and K. Müllen, Chem. Eur. **13**, 6555 (2007).

[4] V. Bulović and S. R. Forrest, Chem. Phys. Lett. **238**, 88 (1995).

[5] D. Kurrle and J. Pflaum, Appl. Phys. Lett. **92**, 133306 (2008).

[6] K. Balakrishnan, A. Datar, T. Naddo, J. Huang, R. Oitker, M. Yen, J. Zhao, and L. Zang, J. Am. Chem. Soc. **128**, 7390 (2006).

[7] B. A. Gregg and R. A. Cormier, J. Phys. Chem. B **102**, 9952 (1998).

[8] S.-G. Liu, G. Sui, R. A. Cormier, R. M. Leblanc, and B. A. Gregg, J. Chem. Phys. B **106**, 1307 (2002).

[9] E. Hädicke and F. Graser, Acta Crystallogr. Sect. C **42**, 189 (1986).

[10] E. Hädicke and F. Graser, Acta Crystallogr. Sect. C **42**, 195 (1986).

[11] G. Klebe, F. Graser, E. Hädicke, and J. Berndt, Acta Crystallogr. Sect. B **45**, 69 (1989).

[12] H.-M. Zhao, J. Pfister, V. Settels, M. Renz, M. Kaupp, V. C. Dehm, F. Würthner, R. F. Fink, and B. Engels, J. Am. Soc. Chem. **131**, 15660 (2009).

[13] A. S. Davydov, *Theory of Molecular Excitons* (Plenum Press, New York, 1971).

[14] I. Vragović and R. Scholz, Phys. Rev. B **68**, 155202 (2003).

[15] J. Mizuguchi and K. Tojo, J. Phys. Chem. B **106**, 767 (2002).

[16] U. Heinemeyer, R. Scholz, L. Gisslén, M. I. Alonso, J. O. Ossó, M. Garriga, A. Hinderhofer, M. Kytka, S. Kowarik, A. Gerlach, and F. Schreiber, Phys. Rev. B **78**, 085210 (2008).

[17] M. H. Hennessy, Z. G. Soos, V. Bulović, and S. R. Forrest, Mat. Res. Soc. Symp. Proc. **488**, 171 (1998).

[18] M. H. Hennessy, Z. G. Soos, R. A. Pascal, and A. Girlando, Chem. Phys. **245**, 199 (1999).

[19] Z. G. Soos, M. H. Hennessy, and G. Wen, Chem. Phys. **227**, 19 (1998).

[20] M. Hoffmann and Z. G. Soos, Phys. Rev. B **66**, 024305 (2002).

[21] L. Gisslén and R. Scholz, Phys. Rev. B **80**, 115309 (2009).

[22] J. S. Briggs and A. Herzenberg, Proc. Phys. Soc. **92**, 159 (1967).

[23] J. S. Briggs and A. Herzenberg, J. Phys. B **3**, 1663 (1970).

[24] C. W. Tang, Appl. Phys. Lett. **48**, 183 (1986).

[25] P. Peumans, A. Yakimov, and S. R. Forrest, J. Appl. Phys. **93**, 3693 (2003).

[26] V. P. Singh, R. S. Singh, B. Parthasarthy, A. Aguilera, J. Anthony, and M. Payne, Appl. Phys. Lett. **86**, 082106 (2005).

[27] F. C. Spano, Annu. Rev. Phys. Chem. **57**, 217 (2006).

[28] J. Mizuguchi, Acta Crystallogr. Sect. C **52**, 2315 (1996).

[29] J. Mizuguchi, Acta Crystallogr. **61**, 1064 (2005).

[30] J. Mizuguchi, Dyes and Pigments **35**, 347 (1997).

[31] S.-B. Rim, R. F. Fink, J. C. Schöneboom, P. Erk, and P. Peumans, Appl. Phys. Lett. **91**, 173504 (2007).

[32] Optical density underlying published absorption coefficient of *trans* PTCBI in Ref. 31, S.-B. Rim and P. Peumans, private communication.

[33] A. D. Becke, Phys. Rev. A **38**, 3098 (1988); C. Lee, W. Yang, and R. G. Parr, Phys. Rev. B **37**, 785 (1988).

[34] A. Schäfer, C. Huber, and R. Ahlrichs, J. Chem. Phys. **100**, 5829 (1994).

[35] R. Ahlrichs, M. Bär, M. Häser, H. Horn, and C. Kölmel, Chem. Phys. Lett. **162**, 165 (1989); [http://www.turbomole.com/].

[36] J. Mizuguchi and N. Shimo, J. Imaging Sci. Technol. **50**, 115 (2006).

[37] J. Mizuguchi, Dyes and Pigments **70**, 226 (2006).

[38] M. D. Halls, J. Velkovski, and H. B. Schlegel, Theor. Chem. Acc. **105**, 413 (2001).

[39] M. Dressel, B. Gompf, D. Faltermeier, A. K. Tripathi, J. Pflaum, and M. Schubert, Opt. Express **16**, 19770 (2008).

[40] E. V. Tsiper and Z. G. Soos, Phys. Rev. B **64**, 195124 (2001).

[41] P. Peumans, S. Uchida, and S. R. Forrest, Nature (London) **425**, 158 (2003).